ACS NANO
Cite This: ACS Nano 2018, 12, 6059–6065
www.acsnano.org
ARTICLE

Ultrashort Carbon Nanotubes That Fluoresce Brightly in the Near-Infrared

Noémie Danné,[†,‡] Mijin Kim,[§] Antoine G. Godin,[†,‡] Hyejin Kwon,[§] Zhenghong Gao,[†,‡] Xiaojian Wu,[§] Nicolai F. Hartmann,[∥] Stephen K. Doorn,[∥] Brahim Lounis,[†,‡] YuHuang Wang,[§,⊥] and Laurent Cognet*[,†,‡]

[†]Laboratoire Photonique Numérique et Nanosciences, Univ. Bordeaux, UMR 5298, F-33400 Talence, France
[‡]Institut d'Optique & CNRS, LP2N UMR 5298, F-33400 Talence, France
[§]Department of Chemistry and Biochemistry, University of Maryland, College Park, Maryland 20742, United States
[∥]Center for Integrated Nanotechnologies, Materials Physics and Applications Division, Los Alamos National Laboratory, Los Alamos, New Mexico 87545 United States
[⊥]Maryland NanoCenter, University of Maryland, College Park, Maryland 20742, United States

Supporting Information

ABSTRACT: **The intrinsic near-infrared photoluminescence observed in long single-walled carbon nanotubes is known to be quenched in ultrashort nanotubes due to their tiny size as compared to the exciton diffusion length in these materials (>100 nm). Here, we show that intense photoluminescence can be created in ultrashort nanotubes (~40 nm length) upon incorporation of exciton-trapping sp^3 defect sites. Using super-resolution photoluminescence imaging at <25 nm resolution, we directly show the preferential localization of excitons at the nanotube ends, which separate by less than 40 nm and behave as independent emitters. This unexpected observation opens the possibility to synthesize fluorescent ultrashort nanotubes—a goal that has been long thought impossible—for bioimaging applications, where bright near-infrared photoluminescence and small size are highly desirable, and for quantum information science, where high quality and well-controlled near-infrared single photon emitters are needed.**

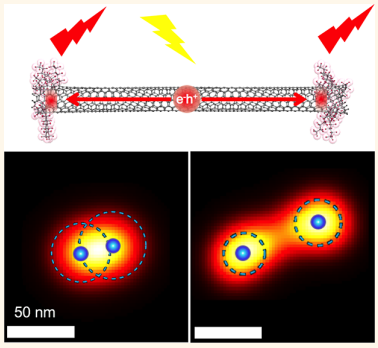

KEYWORDS: *ultrashort carbon nanotube, doping, emission centers, photoluminescence, single molecules, super-resolution microscopy, exciton localization*

The introduction of chemical or structural defects in carbon nanostructures is a powerful route to shape and expand their optical properties. For instance, in nanodiamonds, nitrogen vacancies generate stable photoluminescence, leading to the realization of quantum light sources, sensors, and of promising biological applications.[1−4] More recently, the incorporation of fluorescent quantum defects in single-walled carbon nanotubes (SWCNTs) has created the opportunity to enhance SWCNT near-infrared photoluminescence (PL) properties,[5−8] thus generating a growing interest for the realization of single photon sources and bioimaging fluorophores.[1−4,6,9,10] However, pristine semiconducting SWCNTs display low luminescence quantum yield as their photophysical properties[5−8,11] are mainly imposed by nonradiative mechanisms, associated with structural and environmental defects.[12−16] In this framework, exciton diffusion, which spans typically one to several hundreds of nanometers along the nanotube,[13,17] plays a key role as an exciton scans the integrity of the nanotube backbone before it may eventually emit a photon. As a consequence, ultrashort nanotubes—semiconducting SWCNTs with lengths significantly shorter than the exciton diffusion range—display dominant nonradiative exciton decay mechanisms at the nanotube ends, which are efficient PL quenching sites, leading to imperceptible photoluminescence.[18,19] Due to their exceptional small sizes and near-infrared optical properties, luminescent ultrashort nanotubes would however be a key asset for a variety of applications including nanoelectronics,[20] biology,[21,22] and nanomedicine.[23]

In sp^3-defect-functionalized SWCNTs, recent studies have evidenced the localization of excitons at such defects,[5,24−26] with wide-field PL imaging, suggesting emission from isolated defect sites.[27] However, the extent of localization could not be resolved due to the limited spatial resolution of standard

Received: March 27, 2018
Accepted: June 11, 2018
Published: June 11, 2018

DOI: 10.1021/acsnano.8b02307
ACS Nano 2018, 12, 6059–6065

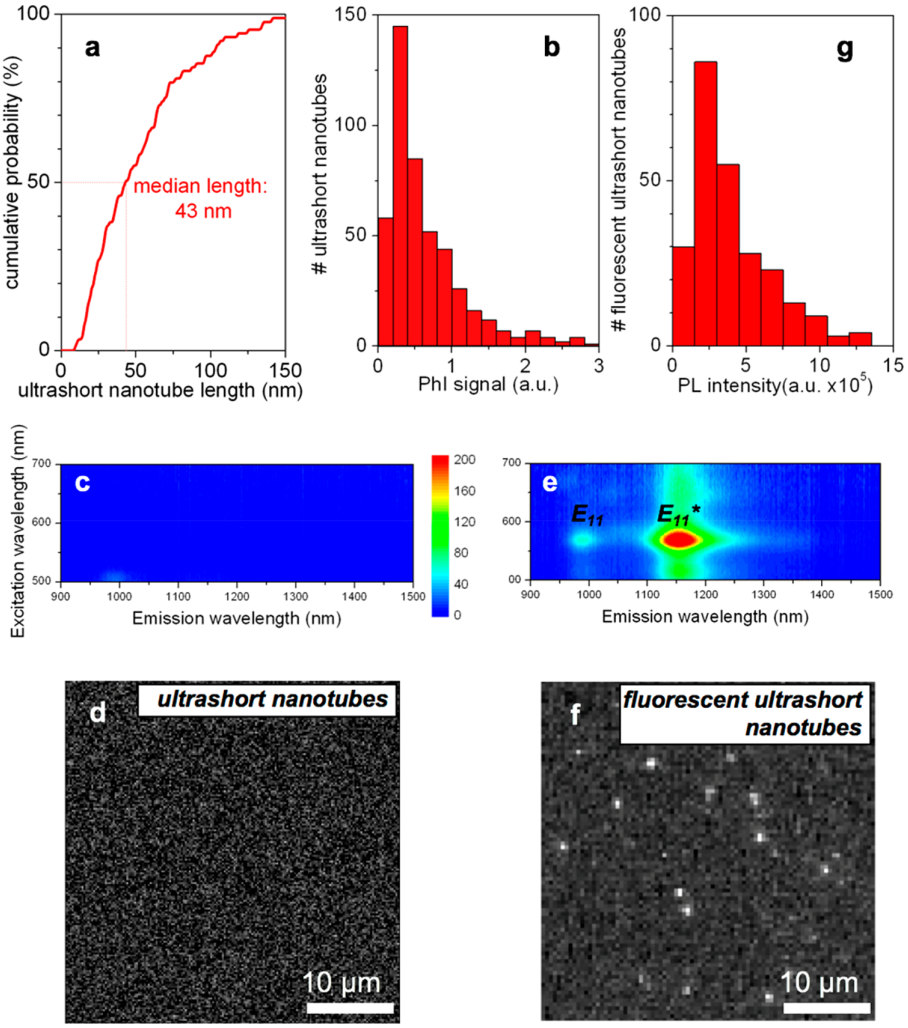

Figure 1. Brightening of ultrashort SWCNTs through fluorescent quantum defects. (a) Cumulative distribution of ultrashort nanotubes lengths measured by AFM (N = 88, median = 43 nm, 1st/3rd quartile = 24/69 nm). (b) Distribution of ultrashort nanotube absorption signals measured by PhI (N = 472), which also reflects the nanotube length distribution but with better statistics. (c) 2D PL map of ultrashort nanotubes shows no luminescence. (d) Single-molecule imaging of ultrashort nanotubes is not observed. (e) 2D PL map of fluorescent ultrashort nanotubes reveals bright luminescence. (f) Single-molecule imaging of fluorescent ultrashort nanotubes is clearly observed. (g) Distribution of fluorescent ultrashort nanotube PL signals (N = 265) mirrors nanotube length distributions in (a) and (b).

microscopy (~450 nm for high numerical aperture (NA) objectives and an emission wavelength of ~1100 nm) as compared to exciton diffusion lengths. Here, we demonstrate that sp^3 defect functionalization can be used to trap excitons at emissive defect sites that are intentionally incorporated into ultrashort nanotubes and thus efficiently brightens ultrashort nanotubes so that it becomes possible to detect them by single-nanotube fluorescence microscopy. Through the application of super-resolution imaging techniques, we further reveal the localization of emitting sites at <25 nm resolution on single ultrashort nanotubes, well below the diffraction limit, size of the nanotubes, and free exciton diffusion lengths. We could then demonstrate that defect sites display independent emission properties, whereas their direct visualization indicates a preferential defect localization at the nanotube ends.

We prepared length-sorted CoMoCAT ultrashort nanotubes featuring a median length of 43 nm following a previously published procedure.[19] The ultrashort lengths were determined by atomic force microscopy (AFM) measurement (N = 88, Figure 1a) and single-particle photothermal imaging (PhI). The photothermal signals are directly linked to nanoparticle absorption so that this distribution mirrors the AFM length measurement, albeit with better statistics[19] (N = 472, Figure 1b). Ensemble absorption spectra confirmed the predominant presence of (6,5) nanotubes in the sample as expected from SG65i CoMoCAT nanotubes (Supporting Information Figure S1). An excitation−emission 2D PL map displayed imperceptible PL signals (Figure 1c), which is not surprising as it has been well-established that ultrashort nanotubes do not fluoresce.[18,19,28] Consistent with the negligible PL in the bulk samples, no luminescent ultrashort nanotubes were detected at the single-nanotube level even using long integration times of several seconds (Figure 1d).

We next covalently attached a perfluorinated hexyl chain ($-C_6F_{13}$) to the ultrashort nanotubes, producing bright photoluminescence in the near-infrared. A 2D PL map of the

DOI: 10.1021/acsnano.8b02307
ACS Nano 2018, 12, 6059−6065

nanotube solution reveals a bright and stable PL peak (E_{11}*) around 1160 nm (Figure 1e). In C_6F_{13}-functionalized, long (6,5)-SWCNTs, this red-shifted peak ($E_{11} - E_{11}$* = 183 meV) has been attributed to PL arising from the chemical functionalization.[8] Interestingly, weak yet photostable E_{11} exciton emission also became observable from fluorescent ultrashort nanotubes, in contrast to the unfunctionalized ultrashort nanotube samples. Fluorescent ultrashort nanotubes that were spin-coated on a microscope glass coverslip precoated with polyvinylpyrrolidone were next observed at the single-tube level. We used a dual detection fluorescence microscope in order to simultaneously detect the E_{11} and/or E_{11}* PL bands of (6,5) fluorescent ultrashort nanotubes upon 568 nm excitation (Supporting Information Figure S2). Unambiguously, bright ultrashort nanotube PL spots could be observed in the E_{11}* channel at the video frame rates (Figure 1f). All detected spots were diffraction-limited as expected from single nanoscale emitters. In addition, we built a distribution of intensities measured from 265 luminescent spots and obtained a monomodal distribution (Figure 1g) in agreement with ultrashort nanotube lengths and PhI signal distributions (Figure 1a,b). These observations reveal that the detected spots stem from individual fluorescent ultrashort nanotubes, and thus that they are bright enough to be detected at the single-tube level owing to C_6F_{13} functionalization. Noteworthy, on occasion, a few dim PL spots were detected in the E_{11} channel and colocalized with E_{11}* PL spots from single fluorescent ultrashort nanotubes (Supporting Information Figure S3), confirming the observation in Figure 1e.

Because ultrashort nanotubes are significantly shorter than the exciton diffusion length (≳100 nm), the efficient PL of fluorescent ultrashort nanotubes is an unambiguous signature of E_{11}* exciton localization (Figure 2). Indeed, the prevailing interpretation for the vanishing E_{11} PL in ultrashort nanotubes is that excitons systematically decay nonradiatively by nanotube ends acting as efficient quenching defects[15,18,29,30] (Figure 2a). C_6F_{13} functionalization thus prevents diffusion-related end quenching of E_{11} excitons through the creation of localized E_{11}* excitons (Figure 2b). Interestingly, the observation of weak yet stable E_{11} PL in fluorescent ultrashort nanotubes might indicate that thermal detrapping of E_{11}* excitons can occur from localized defect sites. In order to investigate the detrapping efficiency, we measured the temperature dependence of the ratio of the E_{11} PL intensity to that of the E_{11}* PL measured in bulk spectra. This ratio follows an Arrhenius-type relation (Figure 3a) with a fitted thermal detrapping energy of 109 meV, which is smaller than the optical gap (183 meV). This energy difference can be understood in terms of the vibrational reorganization energy associated with defect sites.[24] From the Arrhenius law, we estimated that ∼2% of the E_{11}* excitons can be transferred to the E_{11} population through thermal detrapping at room temperature (Figure 3b). However, thermal detrapping cannot fully account for the total observed E_{11} PL in the spectra of fluorescent ultrashort nanotubes. Another mechanism could be that the formation of trapped E_{11}* excitons from photocreated E_{11} excitons requires crossing a small potential barrier[25] (Figure 3c). Finally, all these effects might be reinforced by an E_{11}* state-filling effect, as previously suggested.[31] Indeed, we observed at the single-nanotube level that in fluorescent ultrashort nanotubes, the E_{11}* PL saturates at laser intensities lower than that of E_{11} PL measured on longer unfunctionalized SWCNTs (120 nm median length, Supporting Information

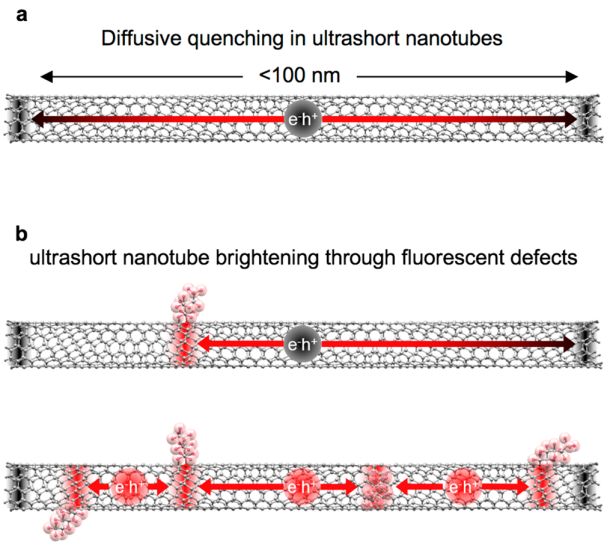

Figure 2. Schematics of photoexcited E_{11} exciton fate in ultrashort nanotubes. (a) Exciton diffusion and quenching in unfunctionalized ultrashort nanotubes. In an ultrashort nanotube, exciton decay is not diffusion-limited but nanotube-length-dependent. End quenching imposes extremely low fluorescence quantum yields of ultrashort nanotubes. (b) Schematics of exciton diffusion and trapping at defects in fluorescent ultrashort nanotubes. Mobile excitons in a fluorescent ultrashort nanotube can be trapped at fluorescent quantum defects and therefore efficiently luminesce (top, one luminescent defect; bottom, multiple defects at different positions).

Figure S4) prepared from the same batch as fluorescent ultrashort nanotubes (Figure 3d,e). Saturation at lower intensities is also consistent with the observation of longer PL decays in sp^3-defect-functionalized SWCNTs as compared to unfunctionalized SWCNTs.[26] Efficient E_{11}* state-filling would then enhance the subpopulation of E_{11} excitons in fluorescent ultrashort nanotubes, resulting in the observed E_{11} emission (Figure 3f). We note that in all these three scenarios (Figure 3b,c,f), the presence of at least two defect sites is required to compete with diffusive quenching at the nanotube ends (Figure 2b).

By preventing E_{11}* excitons from reaching and quenching at the nanotube ends, a single isolated site of sp^3 defect localization can, in principle, brighten ultrashort nanotubes through emission from the defect (1160 nm for (6,5)-SWCNT). It stands to reason that the incorporation of several sites, including at the nanotube ends, should further enhance the photoluminescence (Figure 2b). To determine the relative localization of the defects along the ultrashort nanotubes, the position of emitting sites separated by Δd < 43 nm must be imaged at a resolution much better than the diffraction limit ($1.22\lambda/2NA \sim 500$ nm, for $\lambda = 1160$ nm). This requires a fluorescence imaging modality having at least a 10-fold resolution improvement over standard diffraction-limited fluorescence microscopy. We also wished to investigate whether luminescent defects behave as independent emitters in fluorescent ultrashort nanotubes or whether their close proximity on the nanotube backbone would condition their PL properties.

To achieve the required resolution and considering that emission from fluorescent ultrashort nanotubes occurs in the near-infrared (*i.e.*, at long wavelengths), we implemented a

DOI: 10.1021/acsnano.8b02307
ACS Nano 2018, 12, 6059−6065

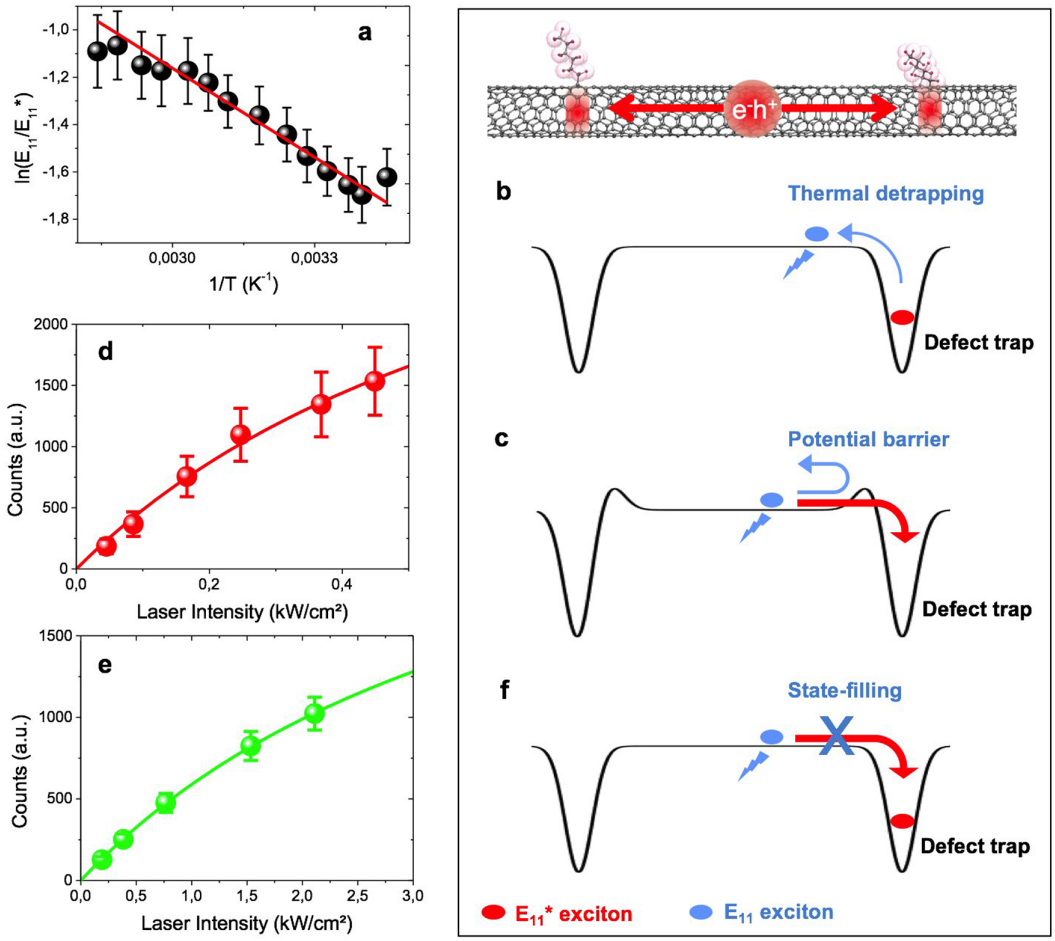

Figure 3. Trapping and detrapping of E_{11}* excitons. (a) van 't Hoff plot for fluorescent ultrashort nanotubes as derived from the integrated PL intensity ratio of E_{11} and E_{11}* at the corresponding temperature (black dots). The slope of the linear fitting (red line) provides the detrapping energy of 109 meV. (b) Schematic representation of thermal detrapping of an E_{11}* exciton to generate a mobile E_{11} exciton. (c) Schematic representation of E_{11}* exciton trapping in the presence of a potential barrier leading to the presence of a small population of E_{11} excitons. (d) Mean E_{11}* PL signal of individual fluorescent ultrashort nanotubes as a function of continuous wave laser intensity (N = 8 ultrashort nanotubes; circles, experimental data; solid line, fit using a saturation profile yielding a saturation intensity of 0.8 kW/cm²). (e) Mean E_{11} PL signal of individual long CNTs from the same preparation as ultrashort nanotubes as a function of continuous wave laser intensity (N = 12 long nanotubes; circles, experimental data; solid line, fit using a saturation profile yielding a saturation intensity of 4.3 kW/cm²). (f) Schematic representation of E_{11}* exciton state filling, leading to the presence of a small population of E_{11} excitons.

super-resolution microscopy strategy based on single emitter localization for its adequacy with the photophysics of fluorescent ultrashort nanotubes—several super-resolution imaging techniques have been widely used in biology to achieve subwavelength resolution imaging in fluorescence microscopy.[32] Localization microscopy was previously demonstrated on pristine SWCNTs, where the nanotubes were exposed to quenching moieties.[33] In the presence of local extrinsic PL, defects were localized as missing PL signals at subwavelength resolution, which also provided a direct visualization of the ∼100 nm exciton excursion range in pristine SWCNTs. Yet, neither ultrashort nanotubes which do not fluoresce nor defect tailored SWCNTs have been previously super-resolved.

In the following, fluorescent ultrashort nanotubes were directly spin-coated on glass coverslips, and single-nanotube PL imaging was performed. In these conditions, the majority of nanotubes showed blinking behavior as similarly observed in long functionalized SWCNTs, probably because of transient defect charging induced by electrostatic interactions at the glass coverslip surface.[27] Figure 4a–d displays PL intensity traces acquired over several minutes, revealing the frequent presence of multiple intensity levels for single fluorescent ultrashort nanotubes. This is quantified by analyzing the amplitude of 64 intensity steps on different nanotubes, presented in the distribution of Figure 4e. The observed distribution of intensity steps is multimodal, with a factor of 2 separating the two subpopulations that we observe, demonstrating that individual sites are imaged in the first subpopulation. Importantly, the presence of the second blinking population indicates that the PL behaviors from two defect sites can be uncorrelated on single (sub-50 nm) fluorescent ultrashort nanotubes. To unambiguously establish the independent localization of defect sites at a length scale on the ultrashort nanotubes and rule out the possibility that nanotube bundles or outliers in nanotube length distribution were at the origin of the second intensity step population, defect localization was investigated by superlocalization

DOI: 10.1021/acsnano.8b02307
ACS Nano 2018, 12, 6059–6065

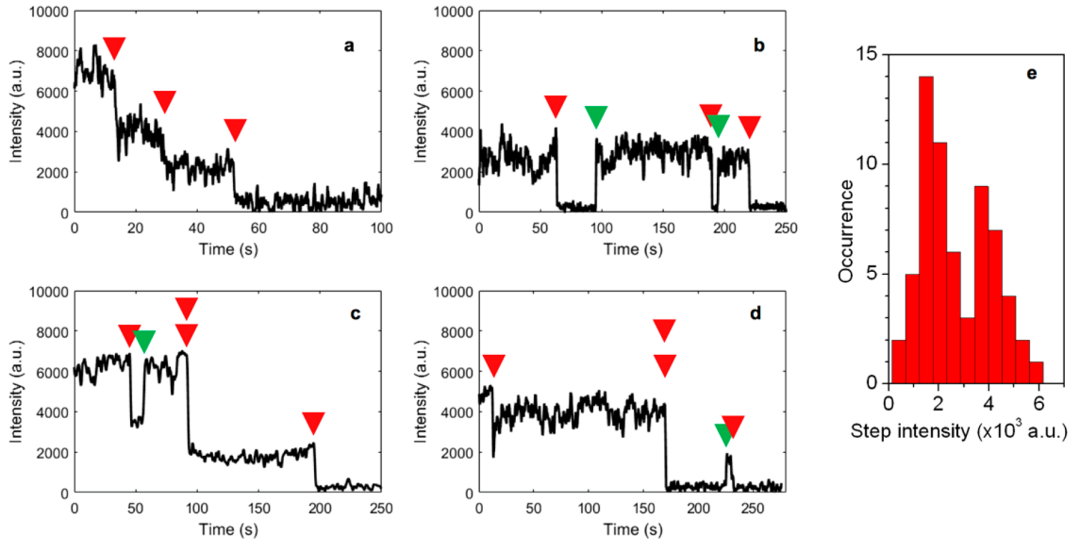

Figure 4. Evidence of E_{11}* exciton localization. (a–d) E_{11}* PL intensity traces of four different single blinking fluorescent ultrashort nanotubes as a function of time. Red (green) triangles represent negative (positive) unitary steps. (e) Histogram of E_{11}* PL step intensities observed in single blinking fluorescent ultrashort nanotubes (N = 64). The histogram is multimodal, which reveals the presence of several individual emitting sites in fluorescent ultrashort nanotubes. The presence of independent intensity levels in fluorescent ultrashort nanotubes having lengths shorter than the diffusion length of E_{11} excitons in long CNTs is a signature of E_{11}* exciton.

analysis on the fluorescent ultrashort nanotubes that displayed multiple intensity steps.

For each intensity step event, differential images were computed, consisting of the differences between successive images before and after the step, in order to isolate the appearance or disappearance of the PL stemming from an individual luminescent site (Figure 5a and Supporting Information Figure S5). When steps were negative, the absolute value of the pixel intensities in the differential image was considered to obtain images with positive pixel values. Images preceding and following the intensity step over time were averaged in order to improve signal-to-noise ratio in the differential images and subsequent localization precision (see Supporting Information methods and Figure S5). Individual spots in differential images were then fitted by a Gaussian approximating the point-spread function as commonly performed in localization microscopy.[34] Indeed, these fits retrieve the locations of individual emitters with subwavelength accuracy.[35] In doing so, we were able to create maps of defect PL localization for several fluorescent ultrashort nanotubes showing more than one intensity level (*i.e.*, at least two independent emitting sites). When background noise can be neglected relative to the number of detected photons (N), the localization precision can be approximated by $\sim s/N^{1/2}$, where s is the standard deviation of the point-spread function. In practice, camera pixelization and noise should be taken into account[36] (see Supporting Information methods), leading to localization precisions that could be estimated for each individual defect site. Taking into account localization precision, on each single nanotube, the detection of defects that were below the localization precision were considered as a single defect (see Supporting Information methods and Figure S6). The mean localization precision for individual defect sites was ultimately determined to be 22 nm in our experiments (see Supporting Information methods). Subsequent defect localizations are shown for several fluorescent ultrashort nanotubes, revealing the presence of at least two unmistakably resolved defects on Figure 5a–e, with localization precision displayed as dotted circles. These images constitute a direct visualization of exciton localization at defect sites to locations below the measured precision, which is significantly smaller than the exciton diffusion range in pristine nanotubes. Interestingly, the distribution of distances between independently localized defects supports this finding (Figure 5f) but also indicates that typical distances between defects match the fluorescent ultrashort nanotube lengths (Figure 1a,b and Figure S7). This observation indicates that functionalization preferentially occurred at nanotube ends (Figure 5g). However, because a small proportion of ultrashort nanotubes are longer than the largest defect separation observed in Figure 5f, it is likely that some sp^3 defects are also randomly localized along nanotube lengths (see example in Figure 5a). We propose that the functionalization reaction occurs propagatively,[37,38] primarily from the nanotube ends which present a large number of quenching defects, and also occasionally from defects present on the backbone of these heavily sonicated ultrashort nanotubes. Functionalization thus creates fluorescent quantum centers[7,8] that prevent excitons generated from the nanotube sp^2 lattice to reach the quenching sites. We therefore believe that the disordered environment at the nanotube ends is reduced by sp^3 defect functionalization.

In this work, we achieved dramatic PL brightening of the normally nonluminescent ultrashort carbon nanotubes by defect functionalization. Brightening is so efficient that the ultrashort carbon nanotubes can be detected at the single-nanotube level. This brightening of sub-100 nm nanotubes is a direct consequence of exciton localization at intentionally introduced defects in the functionalized tubes. To directly observe this mechanism, we developed a super-resolution imaging methodology to resolve the different emission sites with <25 nm resolution on individual nanotubes. Super-resolution imaging suggests that emitting E_{11}* excitons are localized at the nanotube ends. Interestingly, future work might aim at determining the photoluminescence quantum yield of

DOI: 10.1021/acsnano.8b02307
ACS Nano 2018, 12, 6059–6065

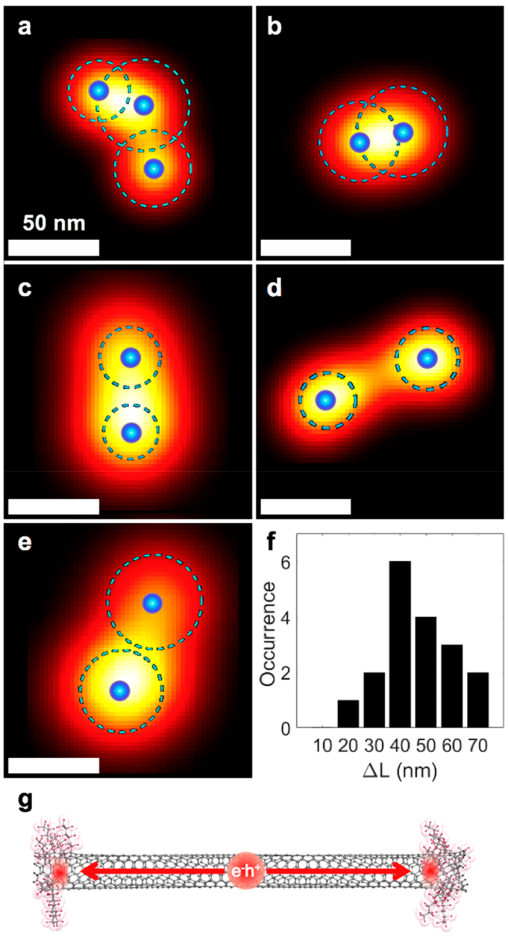

Figure 5. Super-resolved images of E_{11}* exciton localization in fluorescent ultrashort nanotubes. (a−e) Image representation of single blinking E_{11}* exciton localizations in fluorescent ultrashort nanotubes by colored 2D Gaussian curve rendering. For this, each localization is displayed as a two-dimensional Gaussian of unit amplitude and width equal to the localization precision as commonly used in localization microscopy.[34] The mean E_{11}* exciton localization of each single site is represented by blue spots and the corresponding localization precision by dotted circles (see Supporting Information methods and Figure S5). (f) Histogram of super-resolved distances ΔL between E_{11}* exciton localizations (18 fluorescent ultrashort nanotubes were analyzed). (g) Schematic of defect sites preferentially localized at nanotube ends.

luminescent ultrashort nanotubes and will require knowledge of the precise length of the considered ultrashort nanotube to account for its absorption rate as well as the exact number and localizations of sp^3 defects. Brightening of ultrashort nanotubes not only constitutes direct evidence for exciton localization in defect functionalized tubes but also opens a promising route for several applications based on carbon nanotubes. For instance, luminescent ultrashort nanotubes with a controlled number of single emitters might be highly valuable for the development of high-quality single-photon emitters for quantum information applications.[10] We also foresee that upon encapsulation in biocompatible surfactants,[39,40] fluorescent ultrashort nanotubes will constitute a milestone for biological imaging where ultrasmall, bright photostable emitters in the near-infrared biological window are vividly required.[41]

ASSOCIATED CONTENT

Supporting Information

The Supporting Information is available free of charge on the ACS Publications website at DOI: 10.1021/acsnano.8b02307.

Methods section and seven supplementary figures (PDF)

AUTHOR INFORMATION

Corresponding Author

*E-mail: laurent.cognet@u-bordeaux.fr.

ORCID

Nicolai F. Hartmann: 0000-0002-4174-532X
Stephen K. Doorn: 0000-0002-9535-2062
YuHuang Wang: 0000-0002-5664-1849
Laurent Cognet: 0000-0002-3573-5387

Notes

The authors declare no competing financial interest.

ACKNOWLEDGMENTS

This work was supported by CNRS, the French Ministry of Higher Education, Research and Innovation, the Agence Nationale de la Recherche (ANR-14-OHRI-0001-01 and ANR-15-CE16-0004-03), IdEx Bordeaux (ANR-10-IDEX-03-02), and Conseil Regional Nouvelle-Aquitaine (2015-1R60301-00005204). L.C. and B.L. thank the national intrastructure France Bioimaging (ANR-10INS-04-0). Y.H.W. gratefully acknowledges the National Science Foundation of the U.S. for financial support through Grant No. 1507974 for the development of the defect chemistry. The authors thank having had access to the Center for Integrated Nanotechnologies, a U.S. Department of Energy Office of Science user facility.

REFERENCES

(1) Maze, J. R.; Stanwix, P. L.; Hodges, J. S.; Hong, S.; Taylor, J. M.; Cappellaro, P.; Jiang, L.; Dutt, M. V. G.; Togan, E.; Zibrov, A. S.; Yacoby, A.; Walsworth, R. L.; Lukin, M. D. Nanoscale Magnetic Sensing with an Individual Electronic Spin in Diamond. *Nature* **2008**, *455*, 644−647.

(2) Vlasov, I. I.; Shiryaev, A. A.; Rendler, T.; Steinert, S.; Lee, S.-Y.; Antonov, D.; Vörös, M.; Jelezko, F.; Fisenko, A. V.; Semjonova, L. F.; Biskupek, J.; Kaiser, U.; Lebedev, O. I.; Sildos, I.; Hemmer, P. R.; Konov, V. I.; Gali, A.; Wrachtrup, J. Molecular-Sized Fluorescent Nanodiamonds. *Nat. Nanotechnol.* **2014**, *9*, 54−58.

(3) Dolde, F.; Jakobi, I.; Naydenov, B.; Zhao, N.; Pezzagna, S.; Trautmann, C.; Meijer, J.; Neumann, P.; Jelezko, F.; Wrachtrup, J. Room-Temperature Entanglement Between Single Defect Spins in Diamond. *Nat. Phys.* **2013**, *9*, 139−143.

(4) Mochalin, V. N.; Shenderova, O.; Ho, D.; Gogotsi, Y. The Properties and Applications of Nanodiamonds. *Nat. Nanotechnol.* **2012**, *7*, 11−23.

(5) Miyauchi, Y.; Iwamura, M.; Mouri, S.; Kawazoe, T.; Ohtsu, M.; Matsuda, K. Brightening of Excitons in Carbon Nanotubes on Dimensionality Modification. *Nat. Photonics* **2013**, *7*, 715−719.

(6) Ghosh, S.; Bachilo, S. M.; Simonette, R. A.; Beckingham, K. M.; Weisman, R. B. Oxygen Doping Modifies Near-Infrared Band Gaps in Fluorescent Single-Walled Carbon Nanotubes. *Science* **2010**, *330*, 1656−1659.

(7) Piao, Y.; Meany, B.; Powell, L. R.; Valley, N.; Kwon, H.; Schatz, G. C.; Wang, Y. Brightening of Carbon Nanotube Photoluminescence

DOI: 10.1021/acsnano.8b02307
ACS Nano 2018, 12, 6059−6065

Through the Incorporation of sp^3 Defects. *Nat. Chem.* **2013**, *5*, 840−845.
(8) Kwon, H.; Furmanchuk, A.; Kim, M.; Meany, B.; Guo, Y.; Schatz, G. C.; Wang, Y. Molecularly Tunable Fluorescent Quantum Defects. *J. Am. Chem. Soc.* **2016**, *138*, 6878−6885.
(9) Ma, X.; Hartmann, N. F.; Baldwin, J. K. S.; Doorn, S. K.; Htoon, H. Room-Temperature Single-Photon Generation From Solitary Dopants of Carbon Nanotubes. *Nat. Nanotechnol.* **2015**, *10*, 671−675.
(10) He, X.; Hartmann, N. F.; Ma, X.; Kim, Y.; Ihly, R.; Blackburn, J. L.; Gao, W.; Kono, J.; Yomogida, Y.; Hirano, A.; Tanaka, T.; Kataura, H.; Htoon, H.; Doorn, S. K. Tunable Room-Temperature Single-Photon Emission at Telecom Wavelengths From sp^3 Defects in Carbon Nanotubes. *Nat. Photonics* **2017**, *11*, 577−582.
(11) O'Connell, M. J.; Bachilo, S. M.; Huffman, C. B.; Moore, V. C.; Strano, M. S.; Haroz, E. H.; Rialon, K. L.; Boul, P. J.; Noon, W. H.; Kittrell, C.; Ma, J.; Hauge, R. H.; Weisman, R. B.; Smalley, R. E. Band Gap Fluorescence From Individual Single-Walled Carbon Nanotubes. *Science* **2002**, *297*, 593−596.
(12) Perebeinos, V.; Avouris, P. Phonon and Electronic Non-radiative Decay Mechanisms of Excitons in Carbon Nanotubes. *Phys. Rev. Lett.* **2008**, *101*, 057401.
(13) Cognet, L.; Tsyboulski, D. A.; Rocha, J.-D. R.; Doyle, C. D.; Tour, J. M.; Weisman, R. B. Stepwise Quenching of Exciton Fluorescence in Carbon Nanotubes by Single-Molecule Reactions. *Science* **2007**, *316*, 1465−1468.
(14) Berciaud, S.; Cognet, L.; Lounis, B. Luminescence Decay and the Absorption Cross Section of Individual Single-Walled Carbon Nanotubes. *Phys. Rev. Lett.* **2008**, *101*, 077402.
(15) Crochet, J. J.; Duque, J. G.; Werner, J. H.; Lounis, B.; Cognet, L.; Doorn, S. K. Disorder Limited Exciton Transport in Colloidal Single-Wall Carbon Nanotubes. *Nano Lett.* **2012**, *12*, 5091−5096.
(16) Crochet, J. J.; Duque, J. G.; Werner, J. H.; Doorn, S. K. Photoluminescence Imaging of Electronic-Impurity-Induced Exciton Quenching In Single-Walled Carbon Nanotubes. *Nat. Nanotechnol.* **2012**, *7*, 126−132.
(17) Siitonen, A. J.; Tsyboulski, D. A.; Bachilo, S. M.; Weisman, R. B. Surfactant-Dependent Exciton Mobility in Single-Walled Carbon Nanotubes Studied by Single-Molecule Reactions. *Nano Lett.* **2010**, *10*, 1595−1599.
(18) Rajan, A.; Strano, M. S.; Heller, D. A.; Hertel, T.; Schulten, K. Length-Dependent Optical Effects in Single Walled Carbon Nanotubes. *J. Phys. Chem. B* **2008**, *112*, 6211−6213.
(19) Gao, Z.; Oudjedi, L.; Faes, R.; Moroté, F.; Jaillet, C.; Poulin, P.; Lounis, B.; Cognet, L. Optical Detection of Individual Ultra-Short Carbon Nanotubes Enables Their Length Characterization Down to 10 nm. *Sci. Rep.* **2015**, *5*, 17093.
(20) Franklin, A. D.; Luisier, M.; Han, S.-J.; Tulevski, G.; Breslin, C. M.; Gignac, L.; Lundstrom, M. S.; Haensch, W. Sub-10 Nm Carbon Nanotube Transistor. *Nano Lett.* **2012**, *12*, 758−762.
(21) Kolosnjaj-Tabi, J.; Hartman, K. B.; Boudjemaa, S.; Ananta, J. S.; Morgant, G.; Szwarc, H.; Wilson, L. J.; Moussa, F. In Vivo Behavior of Large Doses of Ultrashort and Full-Length Single-Walled Carbon Nanotubes After Oral and Intraperitoneal Administration to Swiss Mice. *ACS Nano* **2010**, *4*, 1481−1492.
(22) Geng, J.; Kim, K.; Zhang, J.; Escalada, A.; Tunuguntla, R.; Comolli, L. R.; Allen, F. I.; Shnyrova, A. V.; Cho, K. R.; Munoz, D.; Wang, Y. M.; Grigoropoulos, C. P.; Ajo-Franklin, C. M.; Frolov, V. A.; Noy, A. Stochastic Transport Through Carbon Nanotubes in Lipid Bilayers and Live Cell Membranes. *Nature* **2014**, *514*, 612−615.
(23) Donkor, D. A.; Tang, X. S. Tube Length and Cell Type-Dependent Cellular Responses to Ultra-Short Single-Walled Carbon Nanotube. *Biomaterials* **2014**, *35*, 3121−3131.
(24) Kim, M.; Adamska, L.; Hartmann, N. F.; Kwon, H.; Liu, J.; Velizhanin, K. A.; Piao, Y.; Powell, L. R.; Meany, B.; Doorn, S. K.; Tretiak, S.; Wang, Y. Fluorescent Carbon Nanotube Defects Manifest Substantial Vibrational Reorganization. *J. Phys. Chem. C* **2016**, *120*, 11268−11276.
(25) Ma, X.; Adamska, L.; Yamaguchi, H.; Yalcin, S. E.; Tretiak, S.; Doorn, S. K.; Htoon, H. Electronic Structure and Chemical Nature of Oxygen Dopant States in Carbon Nanotubes. *ACS Nano* **2014**, *8*, 10782−10789.
(26) Hartmann, N. F.; Velizhanin, K. A.; Haroz, E. H.; Kim, M.; Ma, X.; Wang, Y.; Htoon, H.; Doorn, S. K. Photoluminescence Dynamics of Aryl sp^3 Defect States in Single-Walled Carbon Nanotubes. *ACS Nano* **2016**, *10*, 8355−8365.
(27) Hartmann, N. F.; Yalcin, S. E.; Adamska, L.; Haroz, E. H.; Ma, X.; Tretiak, S.; Htoon, H.; Doorn, S. K. Photoluminescence Imaging of Solitary Dopant Sites in Covalently Doped Single-Wall Carbon Nanotubes. *Nanoscale* **2015**, *7*, 20521−20530.
(28) Cherukuri, T. K.; Tsyboulski, D. A.; Weisman, R. B. Length- and Defect-Dependent Fluorescence Efficiencies of Individual Single-Walled Carbon Nanotubes. *ACS Nano* **2012**, *6*, 843−850.
(29) Hertel, T.; Himmelein, S.; Ackermann, T.; Stich, D.; Crochet, J. Diffusion Limited Photoluminescence Quantum Yields in 1-D Semiconductors: Single-Wall Carbon Nanotubes. *ACS Nano* **2010**, *4*, 7161−7168.
(30) Oudjedi, L.; Parra-Vasquez, A. N. G.; Godin, A. G.; Cognet, L.; Lounis, B. Metrological Investigation of the (6,5) Carbon Nanotube Absorption Cross Section. *J. Phys. Chem. Lett.* **2013**, *4*, 1460−1464.
(31) Iwamura, M.; Akizuki, N.; Miyauchi, Y.; Mouri, S.; Shaver, J.; Gao, Z.; Cognet, L.; Lounis, B.; Matsuda, K. Nonlinear Photoluminescence Spectroscopy of Carbon Nanotubes with Localized Exciton States. *ACS Nano* **2014**, *8*, 11254−11260.
(32) Hell, S. W.; Sahl, S. J.; Bates, M.; Zhuang, X.; Heintzmann, R.; Booth, M. J.; Bewersdorf, J.; Shtengel, G.; Hess, H.; Tinnefeld, P.; Honigmann, A.; Jakobs, S.; Testa, I.; Cognet, L.; Lounis, B.; Ewers, H.; Davis, S. J.; Eggeling, C.; Klenerman, D.; Willig, K. I.; et al. The 2015 Super-Resolution Microscopy Roadmap. *J. Phys. D: Appl. Phys.* **2015**, *48*, 443001.
(33) Cognet, L.; Tsyboulski, D. A.; Weisman, R. B. Subdiffraction Far-Field Imaging of Luminescent Single-Walled Carbon Nanotubes. *Nano Lett.* **2008**, *8*, 749−753.
(34) Godin, A. G.; Lounis, B.; Cognet, L. Super-Resolution Microscopy Approaches for Live Cell Imaging. *Biophys. J.* **2014**, *107*, 1777−1784.
(35) Bobroff, N. Position Measurement with a Resolution and Noise-Limited Instrument. *Rev. Sci. Instrum.* **1986**, *57*, 1152.
(36) Mortensen, K. I.; Churchman, L. S.; Spudich, J. A.; Flyvbjerg, H. Optimized Localization Analysis for Single-Molecule Tracking and Super-Resolution Microscopy. *Nat. Methods* **2010**, *7*, 377−381.
(37) Deng, S.; Zhang, Y.; Brozena, A. H.; Mayes, M. L.; Banerjee, P.; Chiou, W.-A.; Rubloff, G. W.; Schatz, G. C.; Wang, Y. Confined Propagation of Covalent Chemical Reactions on Single-Walled Carbon Nanotubes. *Nat. Commun.* **2011**, *2*, 382.
(38) Zhang, Y.; Valley, N.; Brozena, A. H.; Piao, Y.; Song, X.; Schatz, G. C.; Wang, Y. Propagative Sidewall Alkylcarboxylation That Induces Red-Shifted Near-IR Photoluminescence in Single-Walled Carbon Nanotubes. *J. Phys. Chem. Lett.* **2013**, *4*, 826−830.
(39) Gao, Z.; Varela, J. A.; Groc, L.; Lounis, B.; Cognet, L. Toward the Suppression of Cellular Toxicity From Single-Walled Carbon Nanotubes. *Biomater. Sci.* **2016**, *4*, 230−244.
(40) Gao, Z.; Danné, N.; Godin, A.; Lounis, B.; Cognet, L. Evaluation of Different Single-Walled Carbon Nanotube Surface Coatings for Single-Particle Tracking Applications in Biological Environments. *Nanomaterials* **2017**, *7*, 393.
(41) Godin, A. G.; Varela, J. A.; Gao, Z.; Danné, N.; Dupuis, J. P.; Lounis, B.; Groc, L.; Cognet, L. Single-Nanotube Tracking Reveals the Nanoscale Organization of the Extracellular Space in the Live Brain. *Nat. Nanotechnol.* **2017**, *12*, 238−243.

DOI: 10.1021/acsnano.8b02307
ACS Nano 2018, 12, 6059−6065